AIP Journal of Applied Physics

Ion-implantation-induced amorphization of InxGa1−xP alloys as functions of stoichiometry and temperature

Z. S. Hussain, E. Wendler, W. Wesch, C. S. Schnohr, and M. C. Ridgway

Citation: Journal of Applied Physics **119**, 195702 (2016); doi: 10.1063/1.4950697
View online: http://dx.doi.org/10.1063/1.4950697
View Table of Contents: http://scitation.aip.org/content/aip/journal/jap/119/19?ver=pdfcov
Published by the AIP Publishing

Articles you may be interested in

Lattice damage and compositional changes in Xe ion irradiated InxGa1-xN (x = 0.32−1.0) single crystals
J. Appl. Phys. **119**, 245704 (2016); 10.1063/1.4954691

Structural disorder in ion-implanted Al x Ga 1−x N
Appl. Phys. Lett. **80**, 787 (2002); 10.1063/1.1445478

Polycrystallization and surface erosion of amorphous GaN during elevated temperature ion bombardment
J. Appl. Phys. **88**, 5493 (2000); 10.1063/1.1318361

Defect formation and annealing behavior of InP implanted by low-energy 15 N ions
J. Appl. Phys. **83**, 738 (1998); 10.1063/1.366746

Ion mass and temperature dependence of damage production in ion implanted InP
J. Appl. Phys. **82**, 5965 (1997); 10.1063/1.366499

The new SR865 2 MHz Lock-In Amplifier ... $7950

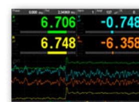
Chart recording

FFT displays

Trend analysis

Features
· Intuitive front-panel operation
· Touchscreen data display
· Save data & screen shots to USB flash drive
· Embedded web server and iOS app
· Synch multiple SR865s via 10 MHz timebase I/O
· View results on a TV or monitor (HDMI output)

Specs
· 1 mHz to 2 MHz
· 2.5 nV/√Hz input noise
· 1 µs to 30 ks time constants
· 1.25 MHz data streaming rate
· Sine out with DC offset
· GPIB, RS-232, Ethernet & USB

SRS Stanford Research Systems
www.thinkSRS.com · Tel: (408)744-9040

Reuse of AIP Publishing content is subject to the terms at: https://publishing.aip.org/authors/rights-and-permissions. Download to IP: 130.56.106.27 On: Thu, 08 Sep 2016 02:10:45

JOURNAL OF APPLIED PHYSICS **119**, 195702 (2016)

Ion-implantation-induced amorphization of $In_xGa_{1-x}P$ alloys as functions of stoichiometry and temperature

Z. S. Hussain,[1,a)] E. Wendler,[2] W. Wesch,[2] C. S. Schnohr,[2] and M. C. Ridgway[1,b)]
[1]*Department of Electronic Materials Engineering, Research School of Physics and Engineering, Australian National University, Canberra, Australian Capital Territory 2601, Australia*
[2]*Friedrich-Schiller-Universität Jena, Institut für Festkörperphysik, Max-Wien-Platz 1, D-07743 Jena, Germany*

(Received 21 February 2016; accepted 25 April 2016; published online 17 May 2016)

Rutherford Backscattering Spectrometry/Channeling and Extended X-ray Absorption Fine Structure measurements have been combined to investigate the amorphization of $In_xGa_{1-x}P$ alloys at 15 and 300 K for selected stoichiometries representative of the entire stoichiometric range. The amorphization kinetics differs considerably for the two temperatures: at 15 K, the amorphization kinetics of $In_xGa_{1-x}P$ is intermediate between the two binary extremes while at 300 K, $In_xGa_{1-x}P$ is more easily amorphized than both InP and GaP. Direct impact and stimulated amorphization both contribute to the amorphization process at 15 K. Dynamic annealing via thermally induced Frenkel pair recombination reduces the influence of direct impact amorphization at 300 K such that the stimulated amorphization is dominant. At this temperature, stimulated amorphization in ternary $In_xGa_{1-x}P$ alloys is supported by the structural disorder inherent from the bimodal bond length distribution. *Published by AIP Publishing.* [http://dx.doi.org/10.1063/1.4950697]

INTRODUCTION

The $In_xGa_{1-x}P$ ternary alloys have attracted attention from the electronics industry as an alternative to $Al_xGa_{1-x}As$ as $In_xGa_{1-x}P$ offers several advantages over $Al_xGa_{1-x}As$. For example, $In_xGa_{1-x}P$ has a much lower reactivity to oxygen which is beneficial for having more reliable devices.[1] Furthermore, the $In_xGa_{1-x}P$ alloys feature one of the widest direct band gaps among the non-nitride III-V semiconductors, enabling applications in the optoelectronics industry[2] particularly as light-emitting diodes. Recently, $In_xGa_{1-x}P$ has also been investigated for possible use in solar cells[3–6] particularly in spatial and terrestrial applications due to increased efficiency and superior radiation resistance.

Like $In_xGa_{1-x}As$, $In_xGa_{1-x}P$ exhibits a bimodal bond-length distribution as predicted theoretically[7] and demonstrated experimentally.[8–10] For $In_xGa_{1-x}As$ implanted at 300 K, we previously reported that the ternary alloys were easier to amorphize than their binary end members[11] and attributed this unanticipated behavior to a stimulated amorphization process, the latter enhanced by the presence of structural disorder resulting from the bimodal bond-length distribution. For this report, we have studied the amorphization kinetics of $In_xGa_{1-x}P$ as functions of both implantation temperature and stoichiometry to determine whether the influence of a bimodal bond-length distribution is particular to $In_xGa_{1-x}As$ or common to other ternary III-V alloys.

Excluding our brief report for $In_{0.64}Ga_{0.36}P$ implanted at 300 K (Ref. 11) and a previous swift heavy ion study,[12] the amorphization kinetics of the $In_xGa_{1-x}P$ alloys has not been investigated. In contrast, the binary end members, InP and GaP, have been studied extensively. For InP, this includes reports from Akano *et al.*[13] who suggested that dynamic annealing during implantation was insignificant below 348 K, Wendler[14] who reported similar results from an investigation of the amorphization as a function of implantation temperature, Bezakova *et al.*[15] who concluded that the amorphization at 77 K could be described as a direct impact process and the overlap of the disordered regions, and Schnohr *et al.*[16] who reported nil differences in the atomic structure of InP amorphized by electronic and nuclear ion-energy loss processes. For GaP, Krynicki *et al.*[17] studied amorphization as functions of ion mass and implantation temperature, reporting a homogeneous amorphization process and an increased influence of dynamic annealing as the ion mass decreased. Direct comparative studies of InP and GaP include Jones and Santana[18] who demonstrated that InP was more easily amorphized than GaP at 77 K and an extensive range of measurements by Wesch *et al.*[19] who compared residual disorder following implantation at 300 K in many of the III-V binary compounds. These and other measurements culminated in an exhaustive review[14] studying the influences of implantation temperature and ion mass, energy, flux, and fluence. Thus, while the amorphization kinetics of the two binary end members, InP and GaP, has been studied extensively[13,15–18,20–24] such is not the case for the $In_xGa_{1-x}P$ ternary alloys. This report thus addresses this shortfall for a material system of scientific importance and technological relevance.

EXPERIMENTAL

Epitaxial $In_xGa_{1-x}P$ layers with $x = 0.34$, 0.50, 0.64, and 0.88 and layer thickness of 1, 2.5, 0.5, and 0.1 μm, respectively, were grown by metal organic chemical vapor deposition

[a)]Author to whom correspondence should be addressed. Electronic mail: zohair.hussain@anu.edu.au
[b)]Deceased, December 2015.

Reuse of AIP Publishing content is subject to the terms at: https://publishing.aip.org/authors/rights-and-permissions. Download to IP: 130.56.106.27 On: Thu, 08 Sep 2016 02:10:45

(MOCVD) on GaAs (100) substrates. The substrates were off-cut by 10° towards the ⟨110⟩ direction to avoid the spinodal decomposition and ordering previously observed in $In_xGa_{1-x}P$ alloys.[25–27] A sacrificial AlAs layer of thickness 0.05 μm was deposited on the GaAs substrate prior to the $In_xGa_{1-x}P$ growth to facilitate sample preparation for the synchrotron-based measurements, as described below.

With the exception of $In_{0.50}Ga_{0.50}P$, all $In_xGa_{1-x}P$ layers were lattice mismatched with the GaAs substrate. Given the layer thicknesses exceeded the critical layer thicknesses reported by Kahn and Ritter,[28] misfit dislocations were generated within the epitaxial layer during the deposition. The influence of this disorder on the amorphization kinetics of $In_xGa_{1-x}P$ was, however, considered insignificant based on the study of the closely related $In_xGa_{1-x}As$/InP material system by Hussain *et al.*[11]

Samples were implanted at 15 and 300 K with 60 keV ^{74}Ge ions using the irradiation facilities of the Friedrich-Schiller-Universität and Australian National University, respectively. The former has the capability of performing Rutherford Backscattering Spectrometry/Channeling (RBS/C) measurements at 15 K,[29] negating the need to warm samples to room temperature and hence eliminating any annealing of implantation-induced disorder over 15–300 K. Post-implantation disorder was quantified with RBS/C using 2 MeV ^{4}He ions and a backscattering angle of 170°. This He ion energy ensures that within the first 200 nm, the In signal is not superimposed by scattering contributions from the other atomic species. The quantity $\Delta\chi_{min}$ (referred to as the difference in minimum yield in the following text) was calculated using $\Delta\chi_{min} = (Y_{implanted} - Y_{unimplanted})/(Y_{random} - Y_{unimplanted})$, where $Y_{implanted}$ and $Y_{unimplanted}$ are the integrated backscattered ion yields in the channeling direction for the implanted and unimplanted sample, respectively, and Y_{random} is the random yield. $\Delta\chi_{min}$ is considered a measure of lattice disorder with a value of 0 corresponding to unimplanted material while a value of 1 represents no epitaxial alignment, consistent with amorphous material. The backscattered ion yield was integrated over a depth range (typically 50–350 Å), where the implantation-induced vacancy production determined from SRIM[30] decreased to two-thirds of the maximum value.

For ease of comparison, the ion fluence N_I was converted to the number of displacements per substrate atom n_{dpa}, where $n_{dpa} = N_{displ}N_I/N_0$. N_{displ} is the number of displacements per ion per unit length calculated with SRIM taking displacement energy of 25 eV for all atomic species. N_0 is the atomic density of the corresponding material. $\Delta\chi_{min}$ data as a function of n_{dpa} were fit using the defect interaction and amorphization model of Hecking[31] and Weber[32] to determine the probabilities for direct impact and stimulated amorphization, P_a and A_s, respectively.

Pre-implantation disorder was quantified with Extended X-ray Absorption Fine Structure (EXAFS) measurements. EXAFS samples were prepared by masking the $In_xGa_{1-x}P$ layer with Apiezon wax for mechanical stability and then dissolving the thin AlAs layer using a 10% $HF:H_2O$ solution as a selective etchant.[33,34] The wax was then dissolved using trichloroethylene and the $In_xGa_{1-x}P$ layer was crushed and mixed with BN for transmission EXAFS measurements as performed at beamline 20-B of the Photon Factory, Japan. EXAFS data were collected at the In and Ga K edges at a temperature of 10–15 K. Structural parameters were determined over a photo-electron wavenumber (k) range of 2–14 Å^{-1} and non-phase-corrected radial distance of 1.5–4.9 Å for the In edge and 1.4–4.6 Å for the Ga edge. Using the IFEFFIT code,[35] the first nearest neighbor (NN) and the next nearest neighbor (NNN) distances were determined, from which the bond angles for each NNN configuration were calculated. A complete multiple scattering analysis was applied.

RESULTS AND DISCUSSION

Ion beam induced damage formation

As an example for the RBS/C spectra measured after ion implantation, Figure 1 plots the spectra of $In_{0.50}Ga_{0.50}P$ ion implanted at room temperature to various ion fluences. In this figure, only the In part of the spectra is shown, which is not superimposed by scattering contributions from the other atomic species. The energy of backscattered ions was converted to depth using the energy loss data as given in the SRIM code. For this particular example, the yield of backscattered ions increases for ion fluences up to 4×10^{13} ions cm^{-2}, where the normalized yield reaches the random level ($\Delta\chi_{min} = 1$). For higher ion fluences, the amorphized layer progressively increases in width. Similar spectra were measured for all the other compounds both at room temperature and at 15 K.

For an implantation temperature of 15 K, Figure 2 shows fits to the difference in minimum yield $\Delta\chi_{min}$ as a function of n_{dpa} over the entire stoichiometry range. For clarity, individual experimental points have been excluded. Fits were done assuming two processes to occur: (i) damage formation (or amorphization) within direct ion impacts with the probability P_a and (ii) stimulated growth of damage (or stimulated amorphization) with probability A_s. These two processes can be represented by a differential equation which is given by

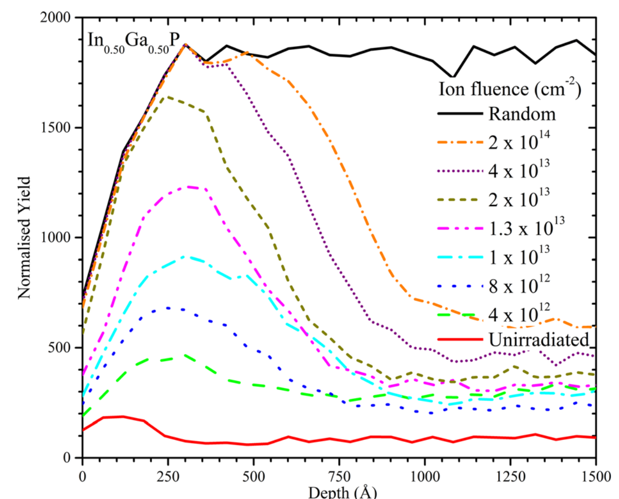

FIG. 1. RBS/C spectra of $In_{0.50}Ga_{0.50}P$ irradiated at 300 K using 60 keV ^{74}Ge ions.

Reuse of AIP Publishing content is subject to the terms at: https://publishing.aip.org/authors/rights-and-permissions. Download to IP: 130.56.106.27 On: Thu, 08 Sep 2016 02:10:45

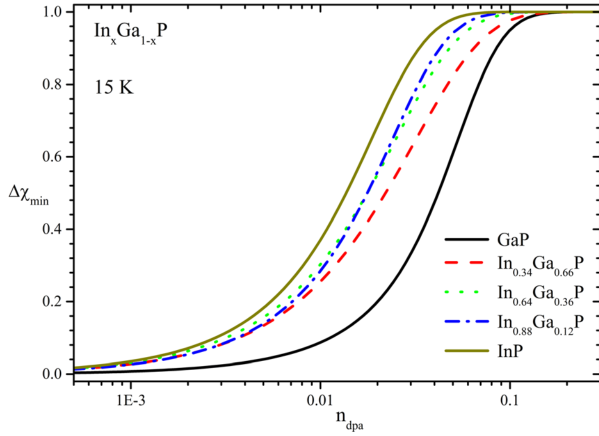

FIG. 2. Difference in minimum yield $\Delta\chi_{min}$ as a function of n_{dpa} measured for $In_xGa_{1-x}P$ at 15 K. The curves are fits to the experimental data points with the latter not shown for clarity.

$$\frac{d\Delta\chi_{min}}{dn_{dpa}} = (P_a + A_s\Delta\chi_{min})(1 - \Delta\chi_{min}). \quad (1)$$

By fitting calculated curves to the measured $\Delta\chi_{min}$ versus n_{dpa} data, values of P_a and A_s were derived. In general, an increase in A_s yields an increase in slope while an increase in P_a shifts the fit to lower n_{dpa} values. As $\Delta\chi_{min}$ approaches unity, the slope of $\Delta\chi_{min}$ versus n_{dpa} approaches zero yielding significant ambiguity in quantifying the n_{dpa} value required for complete amorphization. Given subtle differences in the amorphization kinetics as a function of stoichiometry, we sought to reduce the uncertainty in our comparative study by defining the "critical n_{dpa}" as the inflection point of the fitted curves.

For the two binaries, Figure 2 demonstrates that InP is easier to amorphize than GaP, which is consistent with earlier reports for higher implantation temperatures[14,19] and for other ion species implanted at 15 K.[36]

As one might intuitively expect, the ternary $In_xGa_{1-x}P$ alloys exhibit amorphization kinetics intermediate between the binary end members, which is clearly visible from Figure 2. Similar results have been reported for the ternaries $Al_xGa_{1-x}As$[37] and $In_xGa_{1-x}As$[38] at this low temperature. Figure 3 shows the values of P_a and A_s obtained from fitting of the experimental data. Additionally, values of "critical n_{dpa}" are included, which was introduced above to quantify the amorphization behavior of the alloys. At 15 K, P_a and A_s are roughly similar in magnitude. This means that direct impact amorphization contributes as much as stimulated amorphization to the complete disordering of the implanted layers.

The inset shown in Figure 3 plots the P_a, A_s, and critical n_{dpa} data for 15 K implantation in $In_xGa_{1-x}As$ using the data reported in Ref. 38. Although the probability of stimulated amorphization A_s is larger in $In_xGa_{1-x}As$ and exhibits an opposite trend as a function of the stoichiometry x compared to that observed in $In_xGa_{1-x}P$, there is still a clear indication that both mechanisms, represented by P_a and A_s, contribute to the amorphization process. Moreover, the trend observed for critical n_{dpa} of $In_xGa_{1-x}As$ is similar to that observed for $In_xGa_{1-x}P$, with GaAs being the most difficult to amorphize

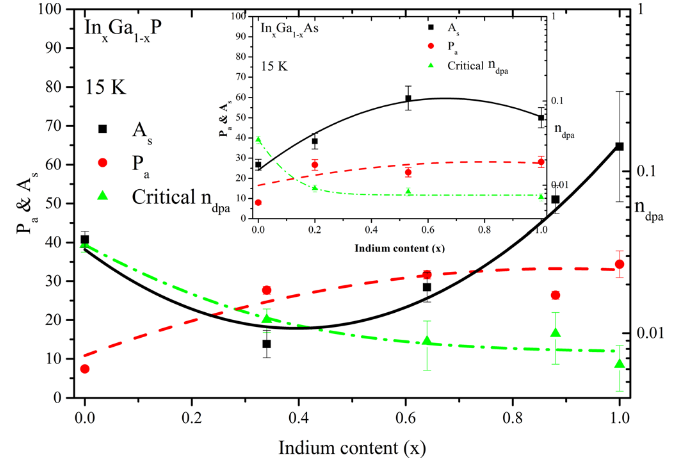

FIG. 3. Critical n_{dpa} and probabilities of direct impact (P_a) and stimulated (A_s) amorphization (in %) as a function of stoichiometry for $In_xGa_{1-x}P$ implanted at 15 K. The inset shows P_a, A_s, and critical n_{dpa} data for $In_xGa_{1-x}As$ implanted at 15 K determined from the data taken from Ref. 38.

and InAs the easiest. Thus, at 15 K, amorphization is driven by both direct impact and stimulated amorphization in both material systems, and $In_xGa_{1-x}P$ and $In_xGa_{1-x}As$ show amorphization kinetics intermediate between those of the binary end members at this temperature.

Figure 4 shows the results from a similar analysis for an implantation temperature of 300 K. Again InP is easier to amorphize than GaP. Note, however, that an increase in critical n_{dpa} by a factor of 8 is required for InP and by a factor of 4 for GaP to amorphize the materials when increasing the implantation temperature from 15 K to 300 K, respectively. In contrast to the amorphization behavior reported above for 15 K, the ternary $In_xGa_{1-x}P$ alloys now do not exhibit amorphization kinetics intermediate between the binary end members. Equivalently, ternary $In_xGa_{1-x}P$ is easier to amorphize than both InP and GaP.

Values of P_a, A_s, and critical n_{dpa} for samples irradiated at 300 K are shown in Figure 5. At this higher temperature, P_a and A_s are no longer comparable as stimulated amorphization now dominates the amorphization process. The direct amorphization component P_a has been reduced by a factor of 4–8 relative to the values at 15 K. In contrast, for the ternary

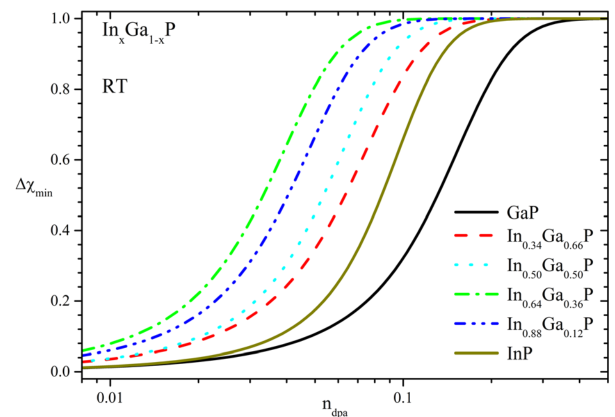

FIG. 4. Difference in minimum yield $\Delta\chi_{min}$ as a function of n_{dpa} measured for $In_xGa_{1-x}P$ at 300 K. The curves are fits to the experimental data points with the latter not shown for clarity.

Reuse of AIP Publishing content is subject to the terms at: https://publishing.aip.org/authors/rights-and-permissions. Download to IP: 130.56.106.27 On: Thu, 08 Sep 2016 02:10:45

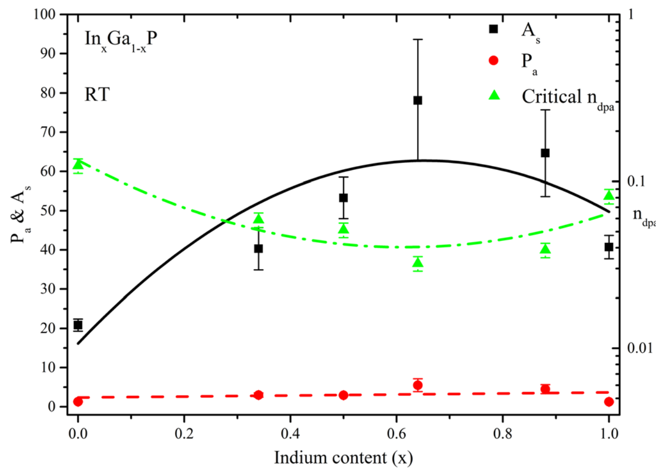

FIG. 5. Critical n_{dpa} and probabilities of direct impact (P_a) and stimulated (A_s) amorphization (in %) as a function of stoichiometry for 300 K implanted $In_xGa_{1-x}P$.

alloys, A_s increases in comparison to the values obtained for ion implantation at 15 K (cp. Figs. 3 and 5). A very similar behavior was previously observed for room temperature implantation of $In_xGa_{1-x}As$.[11] Thus, at 300 K, the crystalline to amorphous transition is dominated by stimulated amorphization in both material systems, and $In_xGa_{1-x}P$ and $In_xGa_{1-x}As$ are more easily amorphized than both their binary end members at this temperature.

Furthermore, the results show that for both temperatures, a systematic change of the transformation to the amorphous phase (cp. Figs. 2 and 4) and of the parameters P_a, A_s, and n_{dpa} (cp. Figs. 3 and 5) occurs with the In content. This supports our assumption that misfit dislocations present in all ternary layers except $In_{0.50}Ga_{0.50}P$ do not significantly influence the amorphization kinetics.

Characterization of the unimplanted alloys

As shown above, the damage formation in the ternary alloys strongly depends on the stoichiometry of the layers. Therefore, more knowledge about the structure of the layers before implantation is required for understanding the observed effects. X-ray absorption spectroscopy provides information about the element specific atomic scale structure of semiconductor compounds and alloys. Therefore, the structural disorder of the as-grown $In_xGa_{1-x}P$ layers before implantation was identified and quantified with EXAFS. Figures 6(a) and 6(b) show non-phase-corrected Fourier-transformed EXAFS spectra of unimplanted InP and $In_{0.50}Ga_{0.50}P$ and unimplanted GaP and $In_{0.50}Ga_{0.50}P$ measured at the In K and Ga K edges, respectively.

An NN peak, due to the scattering from first shell P atoms, is apparent for all samples at a non-phase-corrected radial distance of ~2.1 Å. The amplitude is similar for the ternary and binary alloys, given the NN shell for all three samples is comprised of four P atoms. In contrast, a marked difference in amplitude is observed in the NNN peak at ~3–4.5 Å when comparing the binary and ternary compounds with $In_{0.50}Ga_{0.50}P$ exhibiting a much reduced NNN amplitude compared with InP and GaP. For the binary

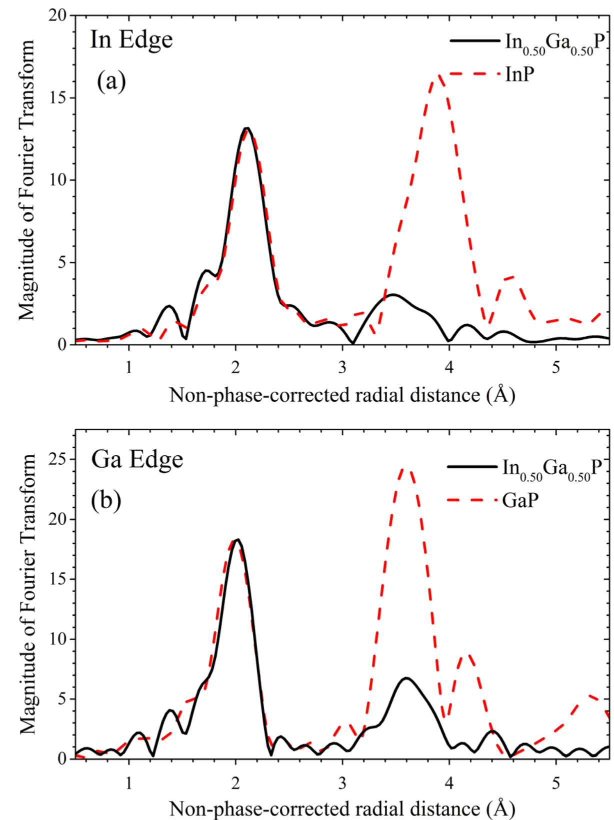

FIG. 6. Fourier transform of EXAFS spectra for (a) crystalline InP and $In_{0.50}Ga_{0.50}P$ as measured at the In K edge and (b) crystalline GaP and $In_{0.50}Ga_{0.50}P$ measured at the Ga K edge.

compounds, the NNN shell consists of 12 In (for InP) or 12 Ga (for GaP) atoms while the NNN shell for $In_{0.50}Ga_{0.50}P$ contains, on average, 6 In and 6 Ga atoms. This reduced NNN peak is characteristic of enhanced structural disorder manifested as an increase in Debye-Waller factor (DWF). As an example of the high quality of the fitting, Figure 7 shows back transformed Ga K edge data for GaP and $In_{0.50}Ga_{0.50}P$, where clearly experiment and theory are well correlated.

Table I lists the bond lengths, bond angles, and DWFs for the binaries and ternaries. Bond length measurements agree well with the previous experimental reports.[8,9]

In-P and Ga-P NN bond lengths, $R_{In\text{-}P}$ and $R_{Ga\text{-}P}$, respectively, are plotted as a function of stoichiometry x in Figure 8. For comparison, a theoretical prediction from the Vegard model, where $R_{In\text{-}P} = R_{Ga\text{-}P}$, is also included. The bond length distribution for the $In_xGa_{1-x}P$ alloys is clearly bimodal with a linear dependence on stoichiometry with the two bond lengths much closer to their respective binary values than to the Vegard model prediction. This bimodal bond length distribution in $In_xGa_{1-x}P$ (and many III-V alloys) can be accommodated by bond stretching, bond bending, or a combination of the two and force constants determine the dominant contribution.[10] Cai and Thorpe[7,39] defined a topological rigidity parameter (a^{**}), where values of 0 and 1 correspond to, respectively, bond stretching only and bond bending only. (The Vegard model is characterized by $a^{**} = 0$.) Following Cai and Thorpe,[7,39] a^{**} values of 0.83 ± 0.07 (In-P) and 0.86 ± 0.07 (Ga-P) were determined from Figure 8. These results are consistent with an average

Reuse of AIP Publishing content is subject to the terms at: https://publishing.aip.org/authors/rights-and-permissions. Download to IP: 130.56.106.27 On: Thu, 08 Sep 2016 02:10:45

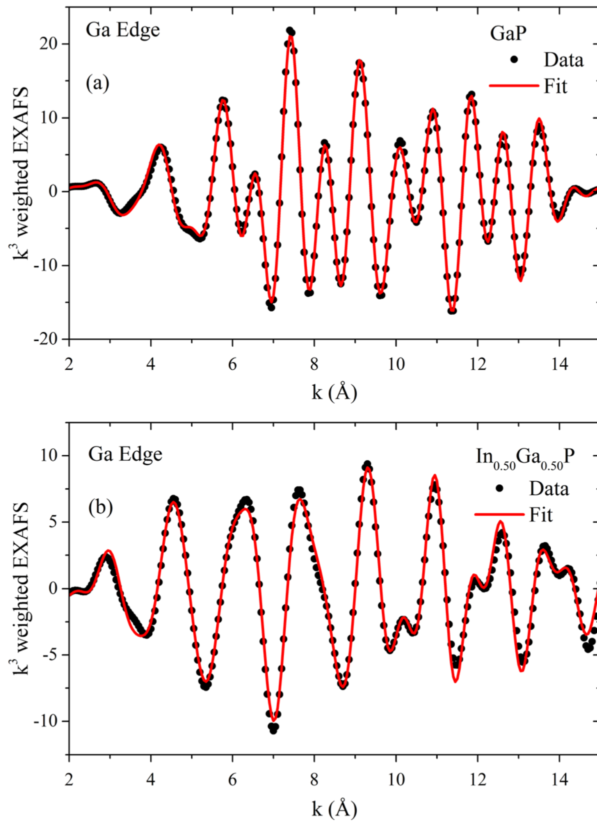

FIG. 7. k^3-weighted back-transformed experimental data versus the photo-electron wave number k for measurements at the Ga K edge for (a) GaP and (b) $In_{0.50}Ga_{0.50}P$.

value of 0.8 reported previously[8,10,40] and indicate that the bimodal bond length distribution in $In_xGa_{1-x}P$ is primarily accommodated by bond bending.

The NNN DWF is influenced by the widths of both the bond length and bond angle distributions while the NN DWF is influenced only by the former. With reference to Table I, note the similarity in NN DWFs for the binaries and ternaries indicative of minimal distortion in the bond length distributions in the alloys. This further supports our claim that the structural disorder in the ternaries is primarily accommodated by bond bending. Table I also shows that the experimentally determined bond angles for the binaries are consistent with the tetrahedral value of 109.5°, as expected. In contrast, the bond angles for the ternaries deviate significantly from this value. The In-P-In bond angle, formed by two (long) In-P bonds, is less than the tetrahedral value, again as expected, while the opposite is true for the Ga-P-Ga bond angle formed by two (short) Ga-P bonds. The value of the In-P-Ga bond angle is 110.2 ± 0.5° which is consistent with the tetrahedral bond angle value.

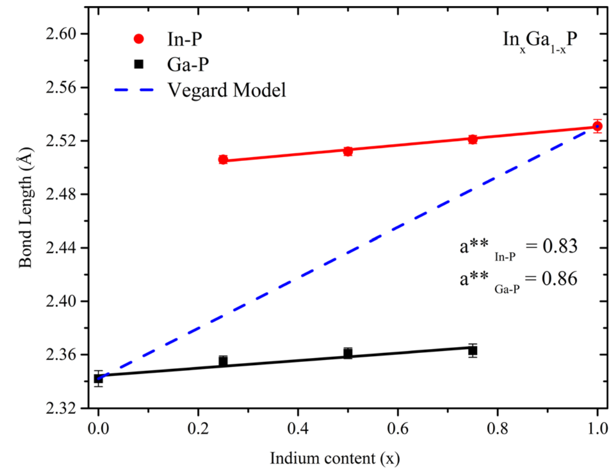

FIG. 8. Nearest-neighbor bond lengths (In-P and Ga-P) for unimplanted $In_xGa_{1-x}P$ as a function of stoichiometry. The Vegard model is included for comparison.

Figure 9 shows the DWF as a function of stoichiometry for the NNN shell about the In atom (In-P-In) and Ga atom (Ga-P-Ga) for $In_xGa_{1-x}P$. Structural disorder at the NNN shell in the ternaries is significantly greater than that of the binaries with a maximum at x = 0.45 +/− 0.27.

Discussion of damage formation

The cross-section (or probability) for damage formation in binary III-V compounds has a systematic dependence on the atomic force constant.[41] This parameter is considered as a measure of bond strength with a higher force constant yielding a lower cross-section for damage formation and, as a consequence, a higher n_{dpa} necessary for amorphization. The lower critical n_{dpa} value for InP compared to GaP observed herein is consistent with the higher force constant of the latter.[41,42] Our results show that this is the case independent of temperature. However, the stronger increase of the critical n_{dpa} and the stronger decrease of P_a with temperature in InP than in GaP

TABLE I. Bond lengths, bond-angles, and Debye Waller factors (DWF) calculated from EXAFS spectra of InP, GaP, and $In_xGa_{1-x}P$.

Material	Bond (NN/NNN)	Bond length (Å) NN	Bond length (Å) NNN	Angle	θ°	DWF_{NN} (10^{-3}) (In-P/Ga-P)	DWF_{NNN} (10^{-3}) (In-P-In/Ga-P-Ga)
GaP	Ga-P/Ga-Ga	2.350 ± 0.003	3.858 ± 0.004	Ga-P-Ga	110.3 ± 0.2	2.7 ± 0.8	4.1 ± 0.3
$In_{0.34}Ga_{0.66}P$	In-P/In-In	2.506 ± 0.003	4.003 ± 0.018	In-P-In	106.0 ± 0.5	2.4 ± 0.3	6.8 ± 1
	Ga-P/Ga-Ga	2.359 ± 0.003	3.920 ± 0.011	Ga-P-Ga	112.4 ± 0.4	2.7 ± 0.4	6.1 ± 1
$In_{0.50}Ga_{0.50}P$	In-P/In-In	2.514 ± 0.003	4.041 ± 0.023	In-P-In	107.0 ± 0.6	2.4 ± 0.3	8 ± 2
	Ga-P/Ga-Ga	2.374 ± 0.003	3.968 ± 0.013	Ga-P-Ga	113.4 ± 0.4	3.0 ± 0.3	6.6 ± 2
$In_{0.66}Ga_{0.34}P$	In-P/In-In	2.523 ± 0.002	4.10 ± 0.01	In-P-In	108.7 ± 0.3	2.5 ± 0.3	6.4 ± 1
	Ga-P/Ga-Ga	2.365 ± 0.003	3.990 ± 0.019	Ga-P-Ga	115.0 ± 0.6	2.7 ± 0.4	5.9 ± 2
InP	In-P/In-In	2.538 ± 0.003	4.157 ± 0.004	In-P-In	110.0 ± 0.2	2.5 ± 0.7	3.8 ± 0.2

Reuse of AIP Publishing content is subject to the terms at: https://publishing.aip.org/authors/rights-and-permissions. Download to IP: 130.56.106.27 On: Thu, 08 Sep 2016 02:10:45

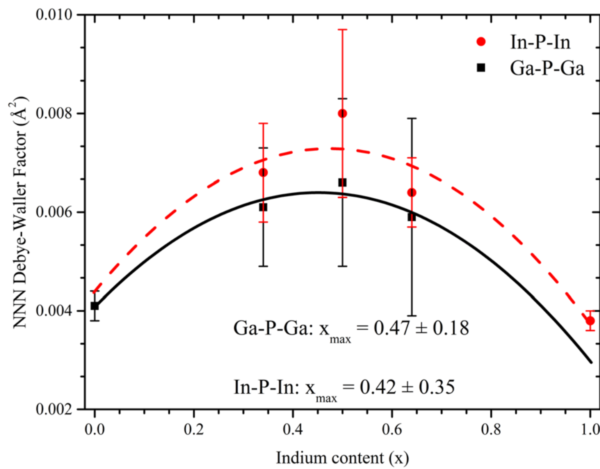

FIG. 9. Debye-Waller factor for the next nearest neighbor in $In_xGa_{1-x}P$ as a function of stoichiometry.

indicates that the influence of temperature on damage formation is stronger in InP than GaP. With increasing temperature, dynamic annealing during the relaxation of the primary collision cascades becomes more prominent. If the dynamic annealing can be characterized by a unique activation energy (E_{act}), our results demonstrate that E_{act}(InP) must exceed E_{act}(GaP). Such an activation energy could well be associated with (irradiation-enhanced) defect mobilities. An enhancement of the defect mobilities may support the recombination of Frenkel pairs and thus the dynamic annealing.

For room temperature ion implantation of $In_xGa_{1-x}P$ alloys, the probability of direct-impact amorphization P_a is effectively independent of stoichiometry x and the values of P_a are rather small (Figure 5). As already explained above for the binary compounds, this can be attributed to dynamical damage annealing. Figure 5 demonstrates that the probability of stimulated amorphization A_s is much larger than P_a. This means that complete amorphization of the implanted layers is dominated by stimulated amorphization. Moreover, the maximum in stimulated amorphization A_s is well correlated with the minimum in critical n_{dpa} with both occurring at an In content of about 0.6. This further demonstrates that A_s is the dominant component in the amorphization process operative at 300 K for the $In_xGa_{1-x}P$ alloys. Equivalently, the differences in critical n_{dpa} value as a function of stoichiometry are governed by the differences in the probability of stimulated amorphization.

When comparing Figures 5 and 9, it is obvious that for implantation at room temperature, A_s exhibits a similar dependence on stoichiometry x as the NNN Debye-Waller factor obtained from the EXAFS analysis. The latter reflects the inherent structural disorder of the as-grown $In_xGa_{1-x}P$ alloys as a result of the bimodal bond length distribution. The maximum observed in structural disorder from EXAFS is well correlated with the maximum observed in stimulated amorphization and the minimum in critical n_{dpa} from RBS/C. Equivalently, the alloy with the lowest n_{dpa} required for amorphization is that with the highest intrinsic structural disorder and the highest probability of stimulated amorphization. This result is in agreement with that observed for room temperature ion implantation in $In_xGa_{1-x}As$.[11] Thus, the influence of a bimodal bond length distribution and associated intrinsic structural disorder on the amorphization process is common to both $In_xGa_{1-x}P$ and $In_xGa_{1-x}As$.[11]

The situation becomes different when the ion implantation is performed at 15 K. The critical n_{dpa} decreases due to reduced dynamic annealing at this low temperature (Figure 3). This is accompanied by a significant increase of probability P_a. In contrast, the values of A_s decrease when decreasing the implantation temperature from 300 K to 15 K for the ternary $In_xGa_{1-x}P$ alloys. For implantation at room temperature, A_s values of the ternary alloys were higher than those of the binaries, whereas at 15 K, they are lower than those of the binaries. These observations demonstrate that at 15 K, amorphization is strongly dominated by direct impact amorphization, whereas stimulated amorphization processes are less important for the ternary $In_xGa_{1-x}P$ alloys. This suggests strong differences in the microscopic mechanisms of amorphization of $In_xGa_{1-x}P$ alloys during ion implantation at room temperature and at 15 K.

In ion implanted $In_xGa_{1-x}As$, both P_a and A_s increase when the implantation temperature is decreased from 300 K to 15 K (see Figure 3 and data in Ref. 11). At both temperatures, P_a is smaller than A_s. And at both temperatures, the dependence of A_s on stoichiometry x resembles that of the NNN DWF, i.e., A_s values of the ternaries are larger than those of the binaries. From these results, it can be suspected that in ion implanted $In_xGa_{1-x}As$, the general mechanisms of amorphization are the same at both temperatures but—due to dynamic annealing—the strength of the processes is reduced for implantation at room temperature.

In general, the ion beam induced, macroscopically measurable transition towards complete amorphization is similar in both the $In_xGa_{1-x}P$ and $In_xGa_{1-x}As$ systems. This is reflected in similar dependencies of the critical n_{dpa} values versus stoichiometry x. However, the results indicate that the microscopic processes which transform the crystalline material into the amorphous state are different in the ternary phosphides and arsenides at 15 K. These differences cannot be explained by the intrinsic disorder due to the bimodal bond length distribution which was measured with EXAFS. Further aspects which may play a role are the by tendency higher force constants of the bonds and the larger values and larger differences in the ionicities of InP and GaP compared to those of InAs and GaAs. However, from the existing experimental results, no satisfying explanation can be given and further investigations are required.

SUMMARY

The kinetics of the ion-implantation-induced amorphization of $In_xGa_{1-x}P$ has been determined over the entire stoichiometry range at temperatures of 15 and 300 K. Strikingly different behavior is apparent at the two temperatures. At 15 K, the probabilities for direct impact and stimulated amorphization are comparable and the amorphization kinetics of the ternary alloys is, as one might expect, intermediate between the binary end members. In contrast, at 300 K, the amorphization kinetics of the ternary alloys is no

Reuse of AIP Publishing content is subject to the terms at: https://publishing.aip.org/authors/rights-and-permissions. Download to IP: 130.56.106.27 On: Thu, 08 Sep 2016 02:10:45

longer intermediate between the binary end members. At this temperature, the direct impact component is reduced by a factor of 4–8 as a result of enhanced Frenkel pair recombination and the stimulated amorphization component is thus dominant. This component is governed by the structural disorder in the $In_xGa_{1-x}P$ alloys that results from the bimodal bond length distribution. The stoichiometry at which the intrinsic disorder is maximum is coincident with the maximum in stimulated amorphization and the minimum in critical n_{dpa} required for amorphization. This behavior is apparent at temperatures (in this case 300 K) where stimulated amorphization is the dominant component in the amorphization process. At low temperatures (in this case 15 K), where the direct impact and stimulated amorphization components are similar, we suggest that the contribution of the former lessens and/or obscures the effect observed at 300 K. Finally, at room temperature, the amorphization process by which ternary alloys are rendered amorphous at n_{dpa} values lower than those required for either of the two binary end members has been demonstrated for $In_xGa_{1-x}P$ and thus is clearly not limited to $In_xGa_{1-x}As$. We suggest this phenomenon should be common to III-V ternary alloys with bimodal bond length distributions with the proviso that the difference in the two bond lengths yields sufficient intrinsic structural disorder.

ACKNOWLEDGMENTS

M.C.R. thanks the Australian Research Council and Australian Synchrotron for financial support and the Australian National Fabrication Facility for access to the ANU implantation facility. W.W. thanks the Group of Eight Australia-Germany Joint Research Cooperation program for financial support.

[1]G.-B. Gao, S. N. Mohammand, G. A. Martin, and H. Morkoc, Int. J. High Speed Electron. Syst. **06**, 1–89 (1995).
[2]J. Novak, S. Hasenhohrl, I. Vavra, and M. Kucera, Appl. Phys. A **87**, 511–516 (2007).
[3]Y. A. Chang, Z. Y. Li, H. C. Kuo, T. C. Lu, S. F. Yang, L. W. Lai, L. H. Lai, and S. C. Wang, Semicond. Sci. Technol. **24**, 085007 (2009).
[4]H. P. T. Nguyen, K. H. Kim, H. Lim, and J. J. Lee, in *International Workshop on Advanced Material for New and Renewable Energy* (2009), Vol. 1169, pp. 149–154.
[5]M. Yamaguchi, Sol. Energy Mater. Sol. Cells **75**, 261–269 (2003).
[6]W. C. Yang, C. Lo, C. Y. Wei, and W. S. Lour, IEEE Electron Device Lett. **32**, 1412–1414 (2011).
[7]Y. Cai and M. F. Thorpe, Phys. Rev. B **46**, 15879–15886 (1992).
[8]J. B. Boyce and J. C. Mikkelsen, J. Cryst. Growth **98**, 37–43 (1989).
[9]C. S. Schnohr, L. L. Araujo, P. Kluth, D. J. Sprouster, G. J. Foran, and M. C. Ridgway, Phys. Rev. B **78**, 115201 (2008).
[10]C. S. Schnohr, Appl. Phys. Rev. **2**, 031304 (2015).
[11]Z. S. Hussain, E. Wendler, W. Wesch, G. J. Foran, C. S. Schnohr, D. J. Llewellyn, and M. C. Ridgway, Phys. Rev. B **79**, 085202 (2009).
[12]C. S. Schnohr, P. Kluth, R. Giulian, D. J. Llewellyn, A. P. Byrne, D. J. Cookson, and M. C. Ridgway, Phys. Rev. B **81**, 075201 (2010).
[13]U. G. Akano, I. V. Mitchell, F. R. Shepherd, and C. J. Miner, Nucl. Instrum. Methods Phys. Res. B **106**, 308–312 (1995).
[14]E. Wendler, Nucl. Instrum. Methods Phys. Res. B **267**, 2680–2689 (2009).
[15]E. Bezakova, A. P. Byrne, C. J. Glover, M. C. Ridgway, and R. Vianden, App. Phys. Lett. **75**, 1923–1925 (1999).
[16]C. S. Schnohr, P. Kluth, A. P. Byrne, G. J. Foran, and M. C. Ridgway, Phys. Rev. B **77**, 073204 (2008).
[17]J. Krynicki, A. Kozanecki, W. Szyszko, and R. Groetzschel, Radiat. Eff. **115**, 219–226 (1990).
[18]K. S. Jones and C. J. Santana, J. Mater. Res. **6**, 1048 (1991).
[19]W. Wesch, E. Wendler, T. Bachmann, and O. Herre, Nucl. Instrum. Methods Phys. Res. B **96**, 290–293 (1995).
[20]V. L. Wrick, W. J. Choyke, and C. F. Tzeng, Electron. Lett. **17**, 752–754 (1981).
[21]E. Wendler, B. Breeger, C. Schubert, and W. Wesch, Nucl. Instrum. Methods Phys. Res. Sect. B **147**, 155–165 (1999).
[22]E. Wendler, in *Application of Accelerators in Research and Industry*, edited by J. L. Duggan and I. L. Morgan (American Institute of Physics, 2003), Vol. 680, pp. 670–674.
[23]R. Dogra, Z. S. Hussain, and A. K. Sharma, Mater. Charact. **58**, 652–657 (2007).
[24]E. Wendler, T. Opfermann, and P. I. Gaiduk, J. Appl. Phys. **82**, 5965–5975 (1997).
[25]M. Kondow, H. Kakibayashi, and S. Minagawa, J. Cryst. Growth **88**, 291–296 (1988).
[26]M. Zorn, P. Kurpas, A. I. Shkrebtii, B. Junno, A. Bhattacharya, K. Knorr, M. Weyers, L. Samuelson, J. T. Zettler, and W. Richter, Phys. Rev. B **60**, 8185–8190 (1999).
[27]F. Léonard and R. Desai, Thin Solid Films **357**, 46–52 (1999).
[28]M. Kahn and D. Ritter, Appl. Phys. Lett. **79**, 2928–2930 (2001).
[29]B. Breeger, E. Wendler, W. Trippensee, C. Schubert, and W. Wesch, Nucl. Instrum. Methods Phys. Res. B **174**, 199–204 (2001).
[30]J. F. Ziegler, Nucl. Instrum. Methods Phys. Res. B **219–220**, 1027–1036 (2004).
[31]N. Hecking, K. F. Heidemann, and E. T. Kaat, Nucl. Instrum. Methods Phys. Res. B **15**, 760–764 (1986).
[32]W. J. Weber, Nucl. Instrum. Methods Phys. Res. B **166**, 98–106 (2000).
[33]Y. Sasaki, T. Katayama, T. Koishi, K. Shibahara, S. Yokoyama, S. Miyazaki, and H. Hirose, J. Electrochem. Soc. **146**, 710 (1999).
[34]S. Decoster, C. J. Glover, B. Johannessen, R. Giulian, D. J. Sprouster, P. Kluth, L. L. Araujo, Z. S. Hussain, C. Schnohr, H. Salama, F. Kremer, K. Temst, A. Vantomme, and M. C. Ridgway, J. Synchrotron Radiat. **20**, 426–432 (2013).
[35]B. Ravel and M. Newville, J. Synchrotron Radiat. **12**, 537 (2005).
[36]E. Wendler and L. Wendler, Appl. Phys. Lett. **100**, 192108 (2012).
[37]B. Breeger, E. Wendler, C. Schubert, and W. Wesch, Nucl. Instrum. Methods Phys. Res. B **148**, 468 (1999).
[38]W. Wesch, E. Wendler, Z. S. Hussain, S. M. Kluth, and M. C. Ridgway, Nucl. Instrum. Methods Phys. Res. B **242**, 480–483 (2006).
[39]Y. Cai and M. F. Thorpe, Phys. Rev. B **46**, 15872 (1992).
[40]J. B. Boyce and J. C. Mikkelsen, *Ternary and Multinary Compounds* (Materials Research Society, Pittsburgh, 1987), p. 359.
[41]E. Wendler and W. Wesch, in *Advances in Solid State Physics*, edited by B. Kramer (Springer-Verlag, 2004), Vol. 44, pp. 339–350.
[42]E. Wendler and W. Wesch, Nucl. Instrum. Methods Phys. Res. B **242**, 562–564 (2006).

Reuse of AIP Publishing content is subject to the terms at: https://publishing.aip.org/authors/rights-and-permissions. Download to IP: 130.56.106.27 On: Thu, 08 Sep 2016 02:10:45